

Terahertz-driven phase transition applied as a room-temperature terahertz detector

C. G. Wade^{1,2,*}, M. Marcuzzi^{3,4}, E. Levi^{3,4}, J. M. Kondo¹, I. Lesanovsky^{3,4}, C. S. Adams¹, and K. J. Weatherill¹

¹*Joint Quantum Centre (JQC) Durham-Newcastle,*

Department of Physics, Durham University, DH1 3LE United Kingdom

²*Clarendon Laboratory, University of Oxford, Parks Road, Oxford OX1 3PU, United Kingdom*

³*School of Physics and Astronomy, University of Nottingham, Nottingham, NG7 2RD, United Kingdom*

⁴*Centre for the Mathematics and Theoretical Physics of Quantum Non-equilibrium Systems,
University of Nottingham, Nottingham NG7 2RD, UK*

There are few demonstrated examples of phase transitions that may be driven directly by terahertz-frequency electric fields, and those that are known require field strengths exceeding 1 MVcm^{-1} . Here we report a room-temperature phase transition driven by a weak ($\ll 1 \text{ Vcm}^{-1}$), continuous-wave terahertz electric field. The system consists of caesium vapour under continuous optical excitation to a high-lying Rydberg state, which is resonantly coupled to a nearby level by the terahertz electric field. We use a simple model to understand the underlying physical behaviour, and we demonstrate two protocols to exploit the phase transition as a narrowband terahertz detector: the first with a fast ($20 \mu\text{s}$) nonlinear response to nano-Watts of incident radiation, and the second with a linearised response and effective noise equivalent power (NEP) $\leq 1 \text{ pWHz}^{-1/2}$. The work opens the door to a new class of terahertz devices controlled with low field intensities and operating around room temperature.

Phase transitions consist of sharp changes in the macroscopic properties of a physical system occurring upon the smooth variation of an external driving parameter (e.g. temperature, electric/magnetic field, ...). The technological applications of phase transitions are diverse, ranging from the storage of energy as latent heat [1], to the action of shape memory alloys [2]. However phase transitions induced by radiation in the terahertz frequency range are rare. Known examples either rely on heating from the terahertz radiation to drive the phase transition indirectly [3], or require electric fields of order 1 MVcm^{-1} that can only be created transiently using pulsed sources [4, 5], limiting their utility. Here we report a phase transition driven directly by a weak, continuous wave (CW) terahertz-frequency field ($\ll 1 \text{ Vcm}^{-1}$), six orders of magnitude smaller than earlier work [4, 5].

The system described in this work consists of an atomic vapour under continuous optical excitation to an energy level with large principal quantum number n , a so-called Rydberg level. Driven-dissipative phase transitions occurring in such media have been a subject of recent experimental [6–8] and theoretical [9–11] interest. The phase transition induces optical bistability and has been associated with the presence of an Ising-like critical point in parameter space [12], while the bistability can be interpreted as a hysteresis cycle across an underlying first-order line [13, 14]. Despite experimental progress [8] further work is needed to fully elucidate the microscopic origin of the phase transition [15] in different parameter regimes. In this work a terahertz-frequency electric field tuned close to a suitable atomic

resonance perturbs the Rydberg bistability, driving the phase transition. By comparing our results with a nonlinear optical-Bloch model, we discriminate between the different mechanisms proposed as the dominating cause of the collective behaviour.

In addition to examining the underlying physical processes, we demonstrate that the abrupt change in system properties in response to a weak terahertz field makes our system suitable as a sensitive terahertz detector. Terahertz devices have seen rapid development in recent decades [16], with new technology based on media from super-conducting [17] and semi-conducting [18] solids to atomic vapour [19–21]. However the traceable calibration of terahertz detectors, typically using cryogenic bolometers, still yields substantial uncertainties [22]. Measurements of atomic properties are easy to reproduce, and therefore lend themselves naturally to measurement standards. Rydberg atoms have recently been used for absolute mm-wave intensity measurements [23, 24], using well-known atomic transition strengths as a reference. Here, by exploiting the phase transition as a terahertz detector we combine the sensitivity afforded by the discontinuous nature of the phase transition, with the ability to calibrate the device in-situ [21].

I. EXPERIMENT

Our experimental system is outlined in figure 1a. The atoms of a thermal caesium vapour are continuously driven to the $21\text{P}_{3/2}$ Rydberg energy level using a three-step ladder laser excitation scheme [25], consisting of probe, coupling and Rydberg lasers (see methods). The vapour is monitored by photographing optical atomic

* christopher.wade@physics.ox.ac.uk

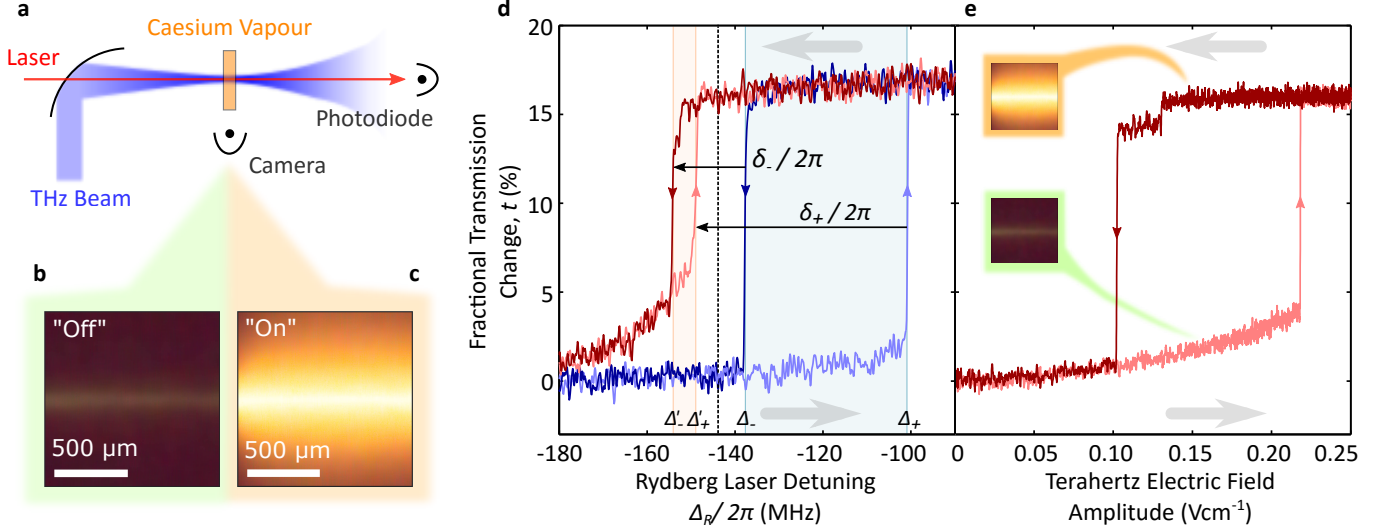


FIG. 1. Experiment Overview: (a) Experiment layout: A room-temperature caesium vapour is continuously excited to a Rydberg energy level by laser driving, and manipulated by a co-axial THz field. The vapour is monitored by measuring laser transmission and atomic fluorescence. (b-c) Photographs of the atomic vapour when it is in the ‘Off’ (b) and ‘On’ (c) steady states. (d) Laser transmission with cycled laser detuning: The hysteretical system response (blue) is altered by the addition of a continuous wave terahertz field with amplitude 0.26 Vcm^{-1} (red). The frequency detuning range for which the response is bistable $\{\Delta_- \leq \Delta_R \leq \Delta_+\}$ shifts to $\{\Delta'_- \leq \Delta_R \leq \Delta'_+\}$, and the shift is parametrised by δ_{\pm} (defined in text). (e) Laser transmission with cycled terahertz power: The laser detuning is held at -145 MHz (vertical dashed line in panel d). The abrupt changes in laser transmission corresponds to the system switching between the ‘Off’ and ‘On’ phases (inset photographs). In panels (d) and (e) the gray arrows indicate the sense of change of the Rydberg laser detuning and the terahertz electric field amplitude respectively.

fluorescence and by measuring the transmitted probe laser power, p , which increases when atoms are shelved in long-lived Rydberg levels or ionised [26]. We use the parameter $t = (p - p_0)/p_0$ to indicate the fractional change in transmitted laser power, where p_0 is the probe laser power transmitted when the Rydberg laser is far off resonance.

By controlling the frequency and intensity of the Rydberg laser, the vapour can be prepared in either of two distinct steady states. The first, which we refer to as ‘Off’, is characterized by the emission of weak green atomic fluorescence (figure 1b) and low probe laser transmission; the second, which we refer to as ‘On’, corresponds to increased probe laser transmission, and bright orange fluorescence (figure 1c). The bright orange fluorescence is due to optical decay from a large selection of Rydberg levels, indicating re-distribution of the atomic population [6, 21]. As the Rydberg laser frequency is scanned we see hysteresis in the response, and the system undergoes abrupt changes as it switches from one state to another (figure 1d) [6, 8]. Denoting positive (blue) laser detuning from the atomic line by $\Delta_R/2\pi$, the transitions from Off-to-On and On-to-Off occur at $\Delta_R = \Delta_+$ and $\Delta_R = \Delta_-$ respectively, making the system bistable for $\Delta_- < \Delta_R < \Delta_+$.

The response is strongly modified when a continuous-wave terahertz-frequency electric field is applied to the

vapour. The field has a frequency of 0.634 THz and resonantly couples the $21P_{3/2}$ Rydberg state to the neighbouring $21S_{1/2}$ level. In particular, when the terahertz field is introduced the bistability window shifts to a new range, $\Delta'_- < \Delta_R < \Delta'_+$, as shown in figure 1d. We define shift parameters, $\delta_- = \Delta'_- - \Delta_-$ and $\delta_+ = \Delta'_+ - \Delta_+$, and we note that in the example shown in figure 1d the hysteresis window shifts and narrows, $\delta_+ < \delta_- < 0$.

In order to demonstrate the terahertz field driving the phase transition directly, we set the laser frequency to the value denoted by the vertical dashed line in figure 1d, and hold all parameters constant while the terahertz electric field amplitude is varied. The vapour is initialised in the ‘Off’ state at zero terahertz field amplitude, and figure 1e shows the response as the terahertz field amplitude is ramped up and then back down again. As the terahertz intensity increases we initially observe a quadratic rise in laser transmission (linear with intensity), before the system switches to the ‘On’ state, indicated by an abrupt increase in t . When the terahertz intensity is decreased again the vapour returns to the ‘Off’ state (accompanied by another sharp change in t), completing the full hysteresis cycle. The hysteresis cycle constitutes a strongly non-linear response of the system to the weak terahertz-frequency electric field.

To characterise the system we map the optical response to the terahertz field in the Rydberg laser- and

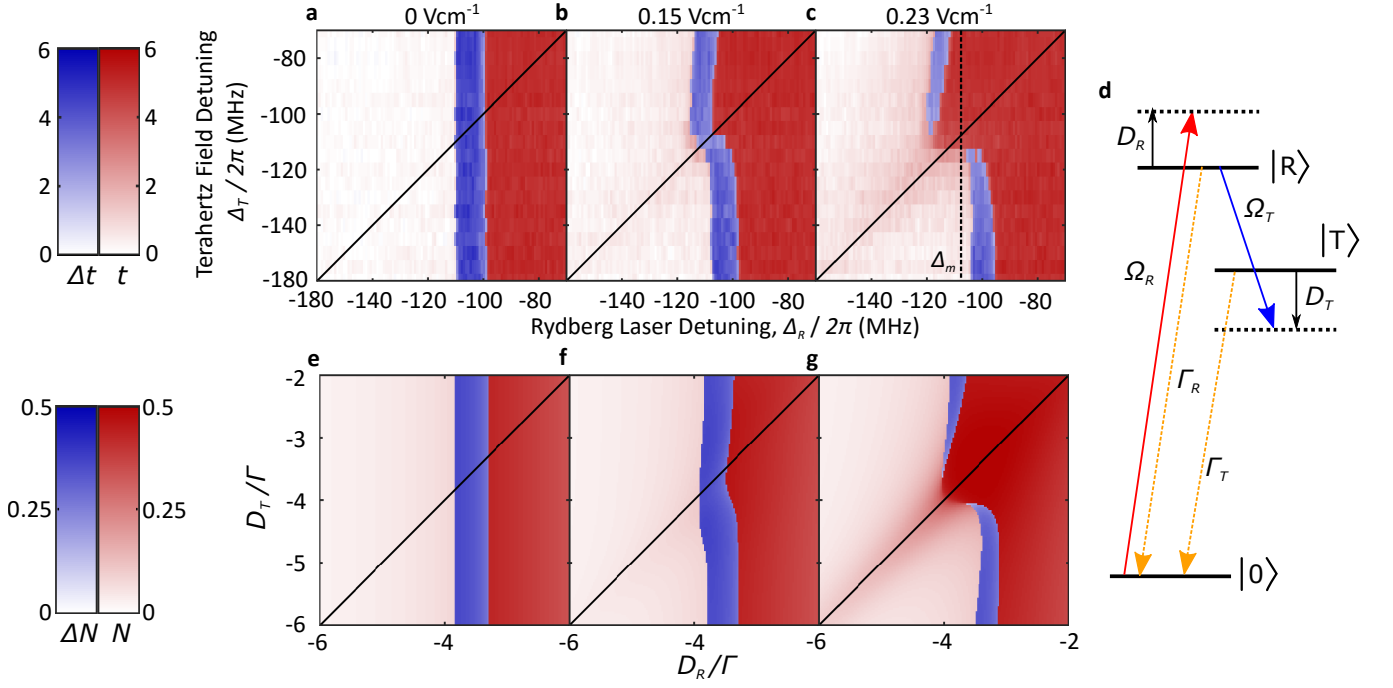


FIG. 2. Experiment and theory comparison: (a-c) Experimental phase maps in laser/terahertz detuning: In areas where the system is monostable (red), we show the fractional increase in laser transmission, t (%). Where the system is bistable (blue) we show $\Delta t = t_{\text{On}} - t_{\text{Off}}$, where t_{On} (t_{Off}) is the fractional transmission change for the ‘On’ (‘Off’) state. In panels a, b and c the terahertz electric field has amplitude $\{0, 0.15, 0.23\}$ Vcm⁻¹ respectively, corresponding to Rydberg transition Rabi frequency $\Omega_T^{\text{meas}}/2\pi = \{0, 31, 48\}$ MHz. The solid black lines show the condition $\Delta_T = \Delta_R$, and the dashed black line in (c) shows the frequency at which the laser could be stabilised in order to demonstrate a reversible latch, $\Delta_R = \Delta_m$, (section III). (d) Theoretical Model: Atoms are excited from $|0\rangle$ to $|R\rangle$ via a laser of Rabi frequency Ω_R and detuning D_R . A second transition takes them from $|R\rangle$ to $|T\rangle$ by means of a terahertz field of corresponding parameters Ω_T and D_T . Excited atoms spontaneously decay to $|0\rangle$ from the two levels $|R\rangle$ and $|T\rangle$ with rates $\Gamma_R = \Gamma_T = 1$. (e-g) Numerically calculated phase maps in laser/terahertz detuning: In areas where the system is monostable (red), we show the sum $N = \langle \sigma_{RR} \rangle + \langle \sigma_{TT} \rangle$ of the excited energy level populations. Where the system is bistable (blue) we show $\Delta N = N_{\text{On}} - N_{\text{Off}}$. The simulation parameters are fixed as follows: $\Omega_R = 1$, $\alpha = -8.3$, $\beta = -5$, $\gamma = \epsilon = 0$, while Ω_T takes the three values 0 (e), 0.3 (f) and 0.8 (g). All parameters are given in units of $\Gamma_R = \Gamma_T \equiv \Gamma$ and are defined in the text.

terahertz-detuning $\{\Delta_R, \Delta_T\}$ plane for a selection of terahertz field amplitudes (figure 2). We describe the response by considering the regions in parameter space where the system is bistable. When the terahertz field is blocked (figure 2a), the bistability region is, as expected, independent of the terahertz field detuning. At intermediate terahertz field strength (0.15 Vcm⁻¹, Rydberg-transition Rabi frequency $\Omega_T^{\text{meas}}/2\pi = 31$ MHz) the bistable parameter space is deformed, and we see that $\delta_{\pm} < 0$ for $\Delta_T > \Delta_R$ and $\delta_{\pm} > 0$ for $\Delta_T < \Delta_R$ (figure 2b). When the field is 0.23 Vcm⁻¹ ($\Omega_T^{\text{meas}}/2\pi = 48$ MHz) the bistable parameter space is split into two separate regions (figure 2c), and we note that bistability becomes absent for all $\Delta_T = \Delta_R$.

II. MEAN-FIELD MODEL

A full simulation of the microscopic dynamics involved in the phase transition is computationally unfeasible,

however previous work has been able to qualitatively describe the Rydberg phase transition using a mean-field model [6, 7]. Here we use a similar model to capture the response of the system to the terahertz field (the full details of which are available in the supplementary information). For simplicity, we start from the optical-Bloch equations for a single atom, and we label $|0\rangle$ the ground state, and $|R\rangle$ and $|T\rangle$ the two Rydberg energy levels, coupled by the THz field (figure 2d). As a first approximation we neglect the two intermediate states used in the experimental ladder excitation scheme, and consider a direct effective coupling between $|0\rangle$ and $|R\rangle$. The coherent part of the evolution is described (in a rotating-wave approximation) by the Hamiltonian

$$\hat{H} = \left[\frac{\Omega_R}{2} \sigma_{0R} + \frac{\Omega_T}{2} \sigma_{RT} + h.c. \right] - D_R \sigma_{RR} - D_T \sigma_{TT}, \quad (1)$$

with $\Omega_{R(T)}$ the effective Rabi frequency of the laser (terahertz field), $D_{R(T)}$ the corresponding detuning, $D_{RT} = D_R - D_T$, and $\sigma_{ab} = |a\rangle \langle b|$ with $a, b \in \{0, R, T\}$.

For the dissipative part, we consider spontaneous decay $|R\rangle \rightarrow |0\rangle$ ($|T\rangle \rightarrow |0\rangle$) at a rate Γ_R (Γ_T). An observable \mathcal{O} then evolves according to the Lindblad equation $\dot{\mathcal{O}} = i[\hat{H}, \mathcal{O}] + \sum_{\alpha=R,T} L_{\alpha}^{\dagger} \mathcal{O} L_{\alpha} - \{L_{\alpha}^{\dagger} L_{\alpha}, \mathcal{O}\}/2$, where the jump operator $L_{\alpha} = \sqrt{\Gamma_{\alpha}} \sigma_{0\alpha}$. In the following, we set $\Gamma_R = \Gamma_T \equiv \Gamma$.

In recent experimental work evidence that the feedback mechanism responsible for the bistable behaviour derives from ionised Rydberg atoms was reported [8]. The study suggests that ions created by inter-atomic collisions generate electric fields within the vapour, which in turn alter the Rydberg excitation rate through Stark shifts of the atomic energy levels. To model the effect of ionisation we assume that a fixed fraction $q_{R(T)}/(1+q_{R(T)})$ of the atoms in energy level $|R(T)\rangle$ spontaneously ionises, producing an ion density $n_{\text{ions}} = q_R \langle \sigma_{RR} \rangle + q_T \langle \sigma_{TT} \rangle$ of ions. We include mean-field shifts of the Rydberg levels $|R(T)\rangle$ in proportion to the ion density, which can be reabsorbed in the detunings via appropriate rescalings

$$\begin{aligned} D_R &\rightarrow D'_R = D_R - \alpha_R n_{\text{ions}}, \\ D_{RT} &\rightarrow D'_{RT} = D_{RT} - \alpha_T n_{\text{ions}}, \end{aligned} \quad (2)$$

where the coefficient $\alpha_{R(T)}$ is proportional to the polarisability of the $|R(T)\rangle$ energy level. We note that the $21S_{1/2}$ state represented by $|T\rangle$ is almost 20 times less polarisable than the $21P_{3/2}$ state represented by $|R\rangle$ [27], and so we make the approximation $\alpha_T \approx 0$.

As an “order parameter”, we focus on the density of excited atoms $N = \langle \sigma_{RR} \rangle + \langle \sigma_{TT} \rangle$, which should provide an effective qualitative comparison to the experimental data, as the transmission t monotonically increases with the number of atoms shelved in the Rydberg energy levels [26]. The calculation results are shown in panels 2(e-g), and we note that the model reproduces several important features of the experimental data: (i) the bistability region appears at negative laser frequency detuning ($\Delta_R < 0$); (ii) the split in the bistability window occurs around the condition $\Delta_R = \Delta_T$ and; (iii) the upper bistability branch experiences a negative shift ($\delta_{\pm} < 0$), whereas the lower one a positive shift ($\delta_{\pm} > 0$). This match was obtained via a numerical scan of the parameters, and the plots in figure 2 correspond to $\alpha_R q_R = -8.3$ and $\alpha_R q_T = -5$ in units of Γ .

The underlying mechanism leading to Rydberg bistability has been a subject of debate. In cold atom ensembles the atomic energy level shifts that lead to Rydberg “blockade” (or “anti-blockade” in the opposite case) [28–31] are caused by dipole interactions, and this mechanism was initially invoked to explain the collective behaviour responsible for the vapour phase transition [6]. However, according to a recent work [15], pure van-der-Waals interactions among excited Rydberg atoms seem to be insufficient to support bistability in a randomly

distributed gas, even when thermal atomic motion prevents the growth of fluctuation correlations. In the development of the mean-field model, we trialled terms in the equations arising from resonant dipole interactions. In the mean-field picture, these pair-wise interactions are incorporated by rescaling,

$$\begin{aligned} D'_R &\rightarrow D''_R = D'_R - \epsilon n_R, \\ D'_{RT} &\rightarrow D''_{RT} = D'_{RT} - \gamma n_T, \end{aligned} \quad (3)$$

where ϵ, γ are phenomenological parameters characterising the strength of the interactions. However, when these terms are dominant ($\alpha_{R(T)} \ll \epsilon, \gamma$) the simulation does not match the behaviour observed in the experiment. Specifically, both branches display a positive shift $\delta_{\pm} > 0$ and, furthermore, if γ is very large then the break in the bistability window does not occur at $\Delta_T = \Delta_R$. This suggests that dipole interactions do not dominate and instead ionisation plays the leading role in the feedback responsible for the phase transition.

III. SENSING APPLICATIONS

The edges of the hysteresis profile constitute sharp spectral features which are sensitive to the presence of the terahertz radiation, and so we propose utilising the collective behaviour as a fast and sensitive way to measure narrowband terahertz radiation. Furthermore the complexity of the phase diagram provides the opportunity to exploit unconventional measurement protocols. In Section I we noted that cycling the terahertz intensity can result in a complete hysteresis loop, however this is not necessarily the case. If the laser frequency is set so that the system is bistable when the terahertz field has zero intensity ($\Delta_- < \Delta_R < \Delta_+$), the hysteresis loop opens and we see a latching response (figure 3a). In this case t increases steadily as the terahertz intensity is ramped up, until the system undergoes the transition to the ‘On’ phase, giving a sharp increase in t . However, if the terahertz field intensity subsequently returns to zero, the transition back to the ‘Off’ state is absent. Instead the system remains in the ‘On’ state for as long as the control parameters do not drift, effectively latching in an altered state. To gain full control of the ‘On’ and ‘Off’ states of the vapour using the terahertz field alone, it would be necessary to stabilise Rydberg laser to a detuning, Δ_m , that divides the two branches of the bistable parameter space when terahertz field is at maximum intensity (indicated by the dashed line in figure 2c). In this circumstance we would expect a pulse of terahertz radiation with $\Delta_T > \Delta_m$ to transfer the system from ‘Off’ to ‘On’ (as we demonstrate with the latching detector configuration), and a pulse with $\Delta_T < \Delta_m$ to reverse the operation, taking ‘On’ back to ‘Off’.

The result of implementing the system as a latching detector is shown in Figure 3b. After the vapour is ini-

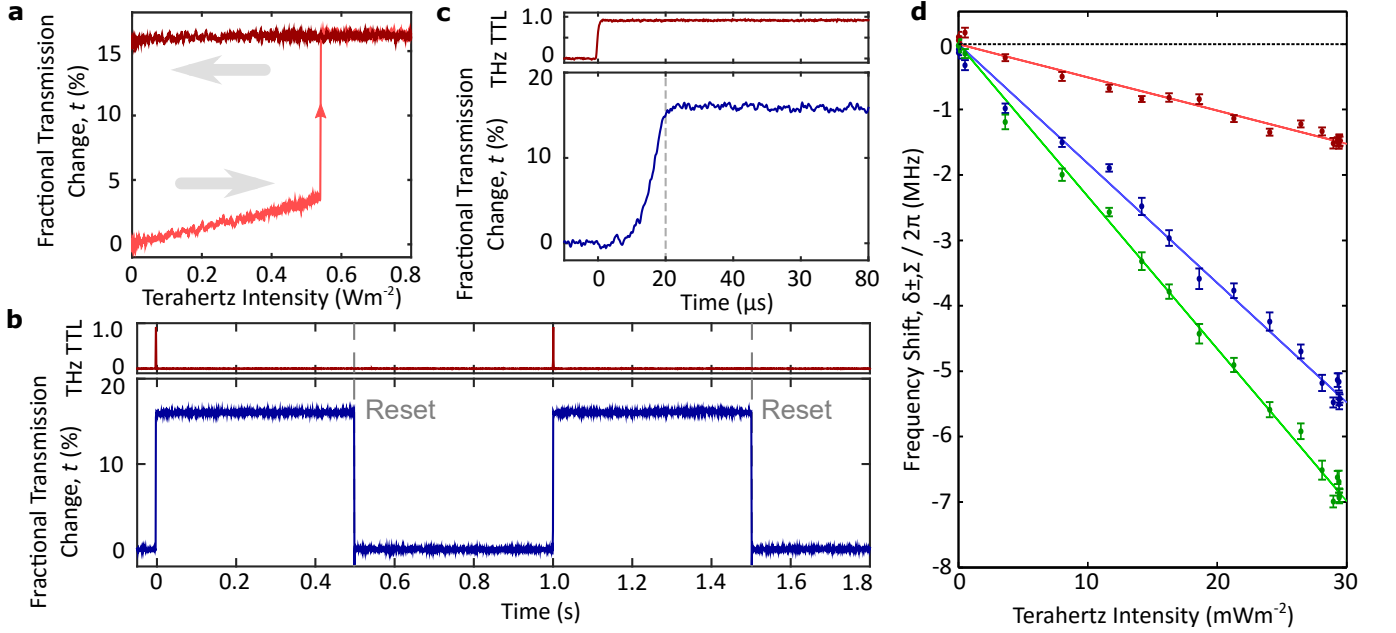


FIG. 3. Sensing configurations: (a) Latching configuration: We show the laser transmission as the terahertz power is cycled (indicated by the gray arrows). Once a critical terahertz intensity has been exceeded the system latches in the ‘On’ state characterised by increased laser transmission. (b) Latching detector protocol: Having initialised the system in the ‘Off’ state, a 1 ms, 0.9 Wm^{-2} terahertz pulse is ‘detected’ and flips the system from ‘Off’ to ‘On’. The system remains in its altered state until the system is reset by cycling the laser power. (c) Latching response time: We show the same latching response on a microsecond timescale. Although the terahertz pulse is constrained to last 1 ms we see that the vapour takes only $20 \mu\text{s}$ to respond. (d) Frequency shift of bistability boundaries: The frequency shifts δ_+ (blue), δ_- (red) and $\Sigma = \delta_+ + \delta_-$ (green) each show a linear dependence on the THz intensity. The error bars show the statistical uncertainty in the mean of 10 or 11 repeated measurements, each lasting 1 ms.

tialised in the ‘Off’ state, a 1 ms, 0.9 Wm^{-2} terahertz pulse is ‘detected’ by the vapour, which switches to the ‘On’ state. The detector is then reset some time later by switching the laser power off for 1 ms. We present measurements of the laser transmission, but the phase transition is also very clear to the eye of an observer, as the vapour fluorescence changes from pale green to bright orange (see figure 1b-c). The 1 ms gate time of the terahertz pulse was as short as we could achieve with our equipment, however this does not reflect the response time of the vapour. When the terahertz field is introduced, the vapour takes only $20 \mu\text{s}$ to switch to the ‘On’ state (figure 3c), indicating that a short period of weak illumination by terahertz radiation can permanently alter the collective state of the system. Taking the sensitive area as the probe laser beam cross section ($1/e^2$ radius $60 \mu\text{m}$), we calculate that a minimum terahertz pulse energy $\approx 200 \text{ fJ}$ is required to latch the vapour. A linear detector attempting to time the arrival of a single 200 fJ , $20 \mu\text{s}$ pulse would require a minimum bandwidth of 50 kHz and a maximum noise equivalent power (NEP) of $50 \text{ pWHz}^{-1/2}$. These requirements can be met comfortably by cryogenically cooled terahertz detectors [32], but stretch the ability of even high-performance room-temperature devices [33–36]. Further work optimising

our experiment control stability would allow the vapour to be biased closer to the phase transition, and therefore require a lower terahertz field intensity to latch the system.

Finally we show how to implement a detector with linear response, which - beyond speed and high sensitivity - is often a desirable property. To linearise the detector output we demonstrate a separate protocol, making use of the frequency shift of the laser detuning range for which the vapour is bistable. We repeatedly scan the Rydberg laser detuning (1 ms per cycle) and read Δ'_{\pm} from each scan. The shifts δ_+ , δ_- and $\Sigma = \delta_+ + \delta_-$ are then calculated using a reference measurement of Δ_{\pm} . With the terahertz detuning set to $\Delta_{\text{T}}/2\pi = -91 \text{ MHz}$ such that $\Delta_{\text{T}} > \Delta_-$, we show the dependence of the shifts on the terahertz intensity in figure 3d (error bars show the standard error in the mean of repeated measurements). The frequency shifts follow a linear relationship with intensity, making intensity (rather than electric field amplitude) the natural sensitivity of the detector (for reference 30 mWm^{-2} is equivalent to 0.048 Vcm^{-1}). By fitting straight lines constrained to pass through the origin [37] we deduce slope coefficients, $m_{\delta_{\pm}, \Sigma}$, which we combine with the average error of the data points, $\bar{\sigma}$

and the measurement time, τ , to find an effective intensity NEP, $\sqrt{\tau\sigma}/m_\Sigma = 48 \pm 3 \mu\text{Wm}^{-2}\text{Hz}^{-1/2}$. Taking the detector area as the probe laser beam cross section yields $\text{NEP} \leq 1 \text{ pWHz}^{1/2}$, though it is not clear how the noise will scale with the laser beam area. Consecutive measurements at 2 ms intervals show no correlation, indicating that the noise present in the system is white in character.

We reference the terahertz field amplitude by making a direct, in-situ measurement of the Rabi-driving frequency of the Rydberg transition driven by the terahertz field. Combining the Rabi frequency with knowledge of the atomic dipole matrix element [27] then allows a calculation of the field amplitude. The measurement is performed by setting the terahertz field detuning to zero ($\Delta_T = 0$) and reading out the frequency interval between a pair of spectral features in the probe laser transmission (Autler-Townes splitting [38]). The result is an absolute measurement of the electric field amplitude, which can be traced directly to fundamental units. The ‘Autler-Townes’ method has been used as a sensitive probe of microwave [39] and terahertz [40] fields in its own right, and techniques such as homodyne measurement [41], frequency modulation spectroscopy [42] and lock-in amplification [39] have been employed to further improve the sensitivity. The results achieved by the Autler-Townes method are now limited by the spectral linewidth of the Rydberg transition and the shot noise of the probe laser [42], which is particularly relevant because the method requires the probe laser to be in the weak excitation regime. Although implementing similar noise reduction techniques in our system will be made complicated by the hysteresis, the collective response produces spectral features (‘Off’ to ‘On’ collective transitions) much narrower than the linewidth of single-atom spectroscopic features, which are limited by the Rydberg atom lifetime. Furthermore the use of bright excitation lasers (necessary for sufficient excited atomic population to see collective behaviour) mitigates the limit imposed by laser shot noise.

IV. CONCLUSION

We have demonstrated a phase transition in a thermal atomic vapour driven by a weak ($\ll 1 \text{ Vm}^{-1}$) terahertz-frequency electric field. The necessary field strength is smaller than reported in other systems by over 6 orders of magnitude [4, 5]. The strong, non-linear response is due to both the inherent inter-particle interactions in the vapour, and the large electric dipole coupling between the Rydberg atoms and the terahertz-frequency field. Non-linear effects induced by terahertz fields have been extensively studied [43], with applications ranging from non-linear spectroscopy [44] and high-harmonic generation [45], to the search for ferroelectric domain switch-

ing [46]. Yet such demonstrations rely on high intensity pulsed terahertz sources. By working in the vicinity of a phase transition we have shown a non-linear response to terahertz radiation in the CW regime, including permanent alteration of the state of the system.

The system can be configured as a narrowband terahertz detector, already showing performance comparable to state-of-the-art room-temperature terahertz detectors [32]. Using an atomic vapour to measure terahertz fields has particular promise because Rydberg terahertz electrometry allows for absolute calibration to SI units through the well known Rydberg atomic dipole moments [24]. Although the requirement to work near an atomic resonance restricts the choice of terahertz frequencies capable of driving such a phase transition, we note that suitable alkali-metal atom Rydberg transitions span the microwave and terahertz frequency regimes, giving thorough coverage [21]. We anticipate further applications combining the phase transition with Rydberg electrometry [39] and Rydberg-fluorescence terahertz imaging [21].

-
- [1] A. Sharma, V. Tyagi, C. Chen, and D. Buddhi, *Renewable and Sustainable Energy Reviews* **13**, 318 (2009).
 - [2] J. M. Jani, M. Leary, A. Subic, and M. A. Gibson, *Materials and Design* **56**, 1078 (2014).
 - [3] D. E. Prober, *Applied Physics Letters* **62**, 2119 (1993).
 - [4] M. Liu, H. Y. Hwang, H. Tao, A. Strikwerda, K. Fan, G. Keiser, A. J. Sternbach, K. West, S. Kittiwatanakul, J. Lu, S. Wolf, F. Omenetto, X. Zhang, K. A. Nelson, and R. D. Averitt, *Nature* **487**, 345 (2012).
 - [5] Z. J. Thompson, A. Stickel, Y.-G. Jeong, S. Han, B. H. Son, M. J. Paul, B. Lee, A. Mousavian, G. Seo, H.-T. Kim, Y.-S. Lee, and D.-S. Kim, *Nano Letters* **15**, 5893 (2015).
 - [6] C. Carr, R. Ritter, C. G. Wade, C. S. Adams, and K. J. Weatherill, *Phys. Rev. Lett.* **111**, 113901 (2013).
 - [7] N. R. de Melo, C. G. Wade, N. Šibalić, J. M. Kondo, C. S. Adams, and K. J. Weatherill, *Phys. Rev. A* **93**, 063863 (2016).
 - [8] D. Weller, A. Urvoy, A. Rico, R. Löw, and H. Kübler, *Phys. Rev. A* **94**, 063820 (2016).
 - [9] T. E. Lee, H. Häffner, and M. C. Cross, *Phys. Rev. Lett.* **108**, 023602 (2012).
 - [10] T. E. Lee, H. Häffner, and M. C. Cross, *Phys. Rev. A* **84**, 031402 (2011).
 - [11] A. Hu, T. E. Lee, and C. W. Clark, *Phys. Rev. A* **88**, 053627 (2013).
 - [12] M. Marcuzzi, E. Levi, S. Diehl, J. P. Garrahan, and I. Lesanovsky, *Physical Review Letters* **113**, 210401 (2014).
 - [13] H. Weimer, *Phys. Rev. Lett.* **114**, 040402 (2015).
 - [14] H. Weimer, *Phys. Rev. A* **91**, 063401 (2015).
 - [15] N. Šibalić, C. G. Wade, C. S. Adams, K. J. Weatherill, and T. Pohl, *Phys. Rev. A* **94**, 011401 (2016).
 - [16] M. Tonouchi, *Nature Photonics* **1**, 97 (2007).
 - [17] S. Cherednichenko, P. Khosropanah, E. Kollberg,

- M. Kroug, and H. Merkel, *Physica C: Superconductivity* **372**, 407 (2002).
- [18] K. Vijayraghavan, Y. Jiang, M. Jang, A. Jiang, K. Choutagunta, A. Vizbaras, F. Demmerle, G. Boehm, M. C. Amann, and M. A. Belkin, *Nature Communications* **4**, 2021 (2013).
- [19] A. Gurtler, A. S. Meijer, and W. J. van der Zande, *Applied Physics Letters* **83**, 222 (2003).
- [20] M. Drabbels and L. D. Noordam, *Applied Physics Letters* **74**, 1797 (1999).
- [21] C. G. Wade, N. Šibalić, N. R. de Melo, J. M. Kondo, K. J. Weatherill, and C. Adams, *Nature Photonics* **72**, 40 (2017).
- [22] L. Werner, H.-W. Hbers, P. Meindl, R. Mller, H. Richter, and A. Steiger, *Metrologia* **46**, S160 (2009).
- [23] M. T. Simons, J. A. Gordon, C. L. Holloway, D. A. Anderson, S. A. Miller, and G. Raithel, *Appl. Phys. Lett.* **108**, 174101 (2016), <http://dx.doi.org/10.1063/1.4947231>.
- [24] M. T. Simons, J. A. Gordon, and C. L. Holloway, *Journal of Applied Physics* **120**, 123103 (2016).
- [25] C. Carr, M. Tanasittikosol, A. Sargsyan, D. Sarkisyan, C. S. Adams, and K. J. Weatherill, *Optics Letters* **37**, 3858 (2012).
- [26] P. Thoumany, T. Hänsch, G. Stania, L. Urbonas, and T. Becker, *Opt. Lett.* **34**, 1621 (2009).
- [27] N. Šibalić, J. Pritchard, C. Adams, and K. Weatherill, *Computer Physics Communications* (2017).
- [28] C. Ates, T. Pohl, T. Pattard, and J. M. Rost, *Phys. Rev. Lett.* **98**, 023002 (2007).
- [29] T. Amthor, C. Giese, C. S. Hofmann, and M. Weidemüller, *Phys. Rev. Lett.* **104**, 013001 (2010).
- [30] I. Lesanovsky and J. P. Garrahan, *Phys. Rev. Lett.* **111**, 215305 (2013).
- [31] I. Lesanovsky and J. P. Garrahan, *Phys. Rev. A* **90**, 011603 (2014).
- [32] F. Sizov and A. Rogalski, *Progress in Quantum Electronics* **34**, 278 (2010).
- [33] H. Qin, J. Sun, S. Liang, X. Li, X. Yang, Z. He, C. Yu, and Z. Feng, *Carbon* **116**, 760 (2017).
- [34] X. He, N. Fujimura, J. M. Lloyd, K. J. Erickson, A. A. Talin, Q. Zhang, W. Gao, Q. Jiang, Y. Kawano, R. H. Hauge, *et al.*, *Nano letters* **14**, 3953 (2014).
- [35] M. S. Vitiello, D. Coquillat, L. Viti, D. Ercolani, F. Teppe, A. Pitanti, F. Beltram, L. Sorba, W. Knap, and A. Tredicucci, *Nano letters* **12**, 96 (2011).
- [36] X. Cai, A. B. Sushkov, R. J. Suess, M. M. Jadidi, G. S. Jenkins, L. O. Nyakiti, R. L. Myers-Ward, S. Li, J. Yan, D. K. Gaskill, *et al.*, *Nature nanotechnology* **9**, 814 (2014).
- [37] I. G. Hughes and T. P. A. Hase, *Measurement and their Uncertainties* (Oxford University Press, 2010).
- [38] S. H. Autler and C. H. Townes, *Phys. Rev.* **100**, 703 (1955).
- [39] J. A. Sedlacek, A. Schwettmann, H. Kübler, R. Löw, T. Pfau, and J. P. Shaffer, *Nature Physics* **8**, 819 (2012).
- [40] M. T. Simons, J. a. Gordon, and C. L. Holloway, in *Terahertz, RF, Millimeter, and Submillimeter-Wave Technology and Applications IX*, Vol. 9747, edited by L. P. Sadwick and T. Yang (2016) p. 97471F.
- [41] S. Kumar, H. Fan, H. Kübler, A. J. Jahangiri, and J. P. Shaffer, *Optics Express* **25**, 8625 (2017).
- [42] S. Kumar, H. Fan, H. Kübler, J. Sheng, and J. P. Shaffer, *Scientific Reports* **7**, 42981 (2017).
- [43] A. Leitenstorfer, K. A. Nelson, K. Reimann, and K. Tanaka, *New Journal of Physics* **16**, 045016 (2014).
- [44] T. Elsaesser, K. Reimann, and M. Woerner, *The Journal of Chemical Physics* **142**, 212301 (2015).
- [45] O. Schubert, M. Hohenleutner, F. Langer, B. Urbanek, C. Lange, U. Huttner, D. Golde, T. Meier, M. Kira, S. W. Koch, and R. Huber, *Nat Photon* **8**, 119 (2014).
- [46] T. Morimoto, T. Miyamoto, H. Yamakawa, T. Terashige, T. Ono, N. Kida, and H. Okamoto, *Phys. Rev. Lett.* **118**, 107602 (2017).

Acknowledgments: The research leading to these results has received funding from: EPSRC (Grants EP/M014398/1, EP/M013103/1 and EP/M013243/1, ‘Networked Quantum Information Technology’ Hub, NQIT); the European Research Council under the European Union’s Seventh Framework Programme (FP/2007-2013) / ERC Grant Agreement No. 335266 (ESCQUMA); FET-PROACT project ‘RySQ’ (H2020-FETPROACT-2014-640378-RYSQ); Durham University; and The Federal Brazilian Agency of Research (CNPq). The authors would like to thank Mike Tarbutt, Andrew Gallant and Claudio Balocco for the loan of equipment, and Nikola Šibalić for stimulating discussions. All data are available on request.

Methods

Atomic Vapour: The caesium is contained in a quartz cell, with laser path length of 2 mm. The temperature of the vapour is stabilised around 70°C using either of two ovens which encase the glass cell, one constructed from stainless steel, the other from *Teflon*. The vapour temperature is inferred by measuring the transmission spectrum of the probe laser [47].

Laser Excitation: We use a three-step excitation process to excite caesium atoms to the Rydberg state. The probe laser (852 nm) excites atoms to the $6P_{3/2}$ state, and the coupling laser (1470 nm) takes the atoms from the $6P_{3/2}$ state to the $7S_{1/2}$. Both the probe and coupling lasers are stabilised to the atomic resonances using polarisation spectroscopy [48]. The Rydberg laser (799 nm) is tuned to the $7S_{1/2}$ to $21P_{3/2}$ state transition, and is stabilised to a reference etalon. All three laser beams are co-axial and the Rydberg laser propagates in the opposite sense to the probe and coupling beams, minimizing the 3-photon Doppler shift due to atomic motion through the optical fields.

Terahertz Beam: The terahertz beam (0.634 THz) is generated from a microwave signal using a amplifier multiplier chain (AMC), manufactured by *Virginia Diodes Inc.*. The beam is linear polarised to match the polarisation of the Rydberg laser and couples the $21P_{3/2}$

state to the $21S_{1/2}$ state. The terahertz beam propagates along the axis of the laser beams.

Automated Control: The main experimental parameters (power and detuning of the Rydberg laser and terahertz beams) are controlled from a computer using a *LabView* program. The microwave source and terahertz AMC are controlled directly through their respective interfaces, and the Rydberg laser frequency is controlled in two ways: For slow frequency scans (figures 1, 2 and

3a) the computer scans the reference etalon to which the Rydberg laser frequency is stabilised. For fast frequency scans (figure 3d) an acousto-optic modulator (AOM) is used instead, however the range is limited to ≤ 100 MHz. The power of the Rydberg laser is controlled using the same AOM. The automated control allowed fast data collection, permitting the data shown in figure 2 to be recorded in only few minutes.

Experimental Parameters: The data were recorded on separate occasions, with parameters summarised as follows:

	Unit	Figure 1, 3a-c	Figure 2	Figure 3d
Vapour temperature	$^{\circ}\text{C}$	71	77	71
Probe laser $1/e^2$ radius	mm	0.06	0.03	0.03
Coupling laser $1/e^2$ radius	mm	0.05	0.10	0.10
Rydberg laser $1/e^2$ radius	mm	0.06	0.13	0.13
Probe laser power	μW	40	70	30
Coupling laser power	μW	60	30	140
Rydberg laser power	mW	330	310	410

[47] M. A. Zentile et al., ElecSus: A program to calculate the electric susceptibility of an atomic ensemble, *Comput. Phys. Commun.* **189** 162 (2015).

[48] C. Carr, K. J. Weatherill and C. S. Adams, Polarization spectroscopy of an excited state transition, *Opt. Lett.* **37** 118 (2012).